Effect of Curved Radial Vane Cavity Arrangements on Predicted Inter-Turbine Burner (ITB) Performance

Hugh Thornburg
Mississippi State University, Mississippi State, MS
hugh.thornburg@wpafb.af.mil

Balu Sekar, Joseph Zelina, and Roger Greenwood
US Air Force Research Laboratory, Propulsion Directorate (AFRL/PR), Turbine Engine Division, Wright-Patterson AFB, OH
{balu.sekar, joseph.zelina, roger.greenwood}@wpafb.af.mil

Abstract

The demand for significantly higher performance gas turbine engines has led to the exploration and identification of "Out of the Box" innovative engine design concepts. These demands include increased thrust-to-weight ratio goals that can primarily be met by substantial engine performance increases such as specific thrust, engine weight and size reductions, and repackaging of engine components to create compact engines. Concepts of an Ultra-Compact-Combustor (UCC) for use as a main combustor, or as an Inter-Turbine Burner (ITB) to boost engine work output, reduce pollutant emissions and engine weight are being explored. The available experimental results and observations indicate that UCC/ITB can operate at 95–99% combustion efficiency over a wide range of operating conditions and with flame lengths up to 50% shorter than those of conventional combustors. In the present study the radial curved vane ITB design concept has been modeled using three-dimensional computational fluid dynamics (CFD). The objectives are to predict ITB flow field and combustion characteristics, guide ITB experimental investigations, identify the key design parameters driving performance, and use the results to optimize ITB design configurations. The CFD predictions demonstrated that intense burning in a high-g loaded cavity occurred which resulted in high combustion efficiency. Models with the radial vane cavity located in both the suction and pressure side have been developed. The circumferential cavity air is injected through the air injection tubes into the circumferential cavity. The orientation of this injection is used to create both a clock-wise (CW) and a counter-clock-wise (CCW) direction of circumferential flow in the outer cavity, when looking upstream from the aft end of the ITB configuration. The resulting five candidate configurations have been simulated and analyzed in detail. This study indicates improved exit profile characteristics for the curved radial vane (CRV) with the cavity in the suction side and the air injected in the CCW direction, compared to the pressure side cavity with air injected either in CCW or CW direction and CRV with no cavity.

1. Introduction

The potential performance benefits of reheat burners placed between turbine stages for propulsion and power generation have been recognized for nearly a century[1-3]. The most common form of reheat is in combined cycle power plants where continuous reheat gas turbines are used to increase efficiency and reduce fuel consumption[4-6]. The augmentor (afterburner) of an aircraft jet engine is another form of reheat after the turbine[7] which is tuned on for only short duration and at certain points in the aircraft's mission profile to provide the required high thrust at these points. As intended, reheat gas turbines ideally operate on a constant temperature (CT) cycle, and as such the CT thermal efficiency is high which makes it very attractive for power extraction for a number of engine applications. Cycle analysis performed by Liu and Sirignano[8-10] using continuous and discrete reheat turbine burners for turbojet and turbofan turbine engines demonstrated clear performance advantages of the reheat cycle as opposed to the conventional non-reheat Brayton cycle in obtaining better specific thrust at a small fractional increase in thrust specific fuel consumption. These studies also pointed out that additional work may be gained if sufficient fuel energy is added to the turbine beyond the main combustor. The performance gain was also found to increase with raising the engine overall operating pressure ratio, bypass ratio, and flight Mach number. These findings reinforce the earlier reheat cycle analysis of Volger[11] for high bypass turbofan engines.

0-7695-3088-5/07 $25.00 © 2007 IEEE

Thermodynamic cycle analysis conducted by Andriani, et al.[12], for augmented thrust engine showed that constant temperature burning throughout the turbine is superior to an augmented thrust engine in terms of both specific thrust and specific fuel consumption.

Significant work increase in the cycle from the reheat burners may be achieved with a relatively small ΔT rise across the reheat burners provided that total pressure drop and Rayleigh losses are minimized. However, the success of the reheat and/or ITB for gas turbine engines hinges on a number of characteristics such as the length, rate of heat release, combustion efficiency, emission levels, and turbine durability. A short ITB, for instance, would be required so that the engine weight is not appreciably increased. However, as the ITB overall length is shortened, complete liquid spray atomization, heating, vaporization, mixing of fuel and air, and combustion becomes very challenging, given the combustor weight and volume constraints. As these combustors become shorter, fuel-air mixture residence time in the combustor is reduced. This increased the potential for incomplete combustion, which is associated with large quantities of partially oxidized fuels such as CH_4, C_2H_4, C_3H_6, and CO. For a combustor, the unburned fuels would flow into the high pressure turbine (HPT). For an ITB placed between the turbine stages, the unburned fuels would enter the low pressure turbine. In each case, the fuels would mix with the cooling air and combust on turbine hardware surfaces with potential for catastrophic failure of the turbine. To reconcile such conflicting performance, emission, and hot section life requirements, identifying revolutionary high payoff UUC/ITB concepts becomes critical.

Recently, a novel ITB concept, which employs an innovative fueled-cavity type flame holder with an angled injection of air from the outer casing in a turbine vane and is situated between the HPT and low pressure turbine (LPT) stages to produce additional thrust has been envisioned by the Air Force Research Laboratory (AFRL)[13-16] and is briefly described here. Figure 1 shows the baseline ITB. This baseline configuration has a cavity, runs around the outer circumference of the vanes. Aligned with this cavity, within each vane, will be a radial vane cavity (RVC). The idea is to burn rich in the circumferential cavity, allowing much of the required combustion residence time to take place in the circumferential direction of the engine, rather than the axial as is done in conventional combustors. Flame stabilization occurs as combustion products are recirculated in the cavity. The intermediate products of combustion will be transported into the RVC where combustion will continue at a reduced equivalence ratio. This baseline concept has been extensively studied both numerically and experimentally[17-21].

Concurrently with the testing efforts, three-dimensional (3D) CFD computations have been carried out to guide the experiments, assist in the down select process for the best performing design configuration, and to optimize the selected concept for maximum performance. The overall objective of this work is to numerically model the ITB design with the curved RVC with Jet-A fuel spray injection. The Jet-A liquid fuel spray injected into the circumferential cavity is subjected to aerodynamic forcing from the high g-loading of the air flow which leads to primary and secondary spray break-up along with the formation of ligaments and droplets. The fuel vapor produced by the vaporization of the spray droplets is mixed with the cavity air flow and combusted. The combustion process may either be complete or incomplete by the time the combustion products flow into the RVC, depending upon the degree of fuel-air mixing, the available time for combustion in the cavity, and the amount of unburned fuel shedding out of the circumferential cavity into the main airflow. In addition, the location at which the combustion products shed from the RVC and the level of mixing of these products with main airflow determines what the low pressure turbine would see in terms of radial profiles and pattern factor. Accurate modeling of the complex spray, mixing, and combustion processes is, therefore critical for pre-test predictions to augment and guide experimental efforts and for detailed post-test analysis in the development of a viable UCC/ITB.

2. Simulation Approach

In the present study, a 3D solid model of the UCC/ITB was provided to define the geometry and served as the staring point for this effort. FLUENT version 6.3.26[22] has been utilized for simulations presented. Fluent provides a wide range of physical models and mesh composition flexibility. For example, the discrete phase modeling capability is needed to model the transition of liquid fuel spray into gas-phase employing both Eularian and Lagrangian frames of reference. In the next section the details of the combustion model used in this study; the spray representation of the Jet-A, the various boundary conditions, the numerical integration scheme, the computational grid, and the CFD results are given.

3. Combustion Model

In general, numerical modeling of the combustion process requires detailed and/or reduced chemical reaction mechanisms for adequate accuracy. In the present study, Jet-A fuel chemistry is modeled by using a simplified one-step irreversible chemical reaction scheme given below as

$$4\,C_{12}H_{23} + 71\,O_2 + N_2 \rightarrow 48\,CO_2 + 46\,H_2O + N_2 \qquad (1)$$

It is important to note here that the purpose of utilizing a single reaction step at this point of UCC/ITB technology evaluation is to simplify the CFD computations and obtain overall global combustion features in the ITB such as finite-rate flame length, combustion heat release, and ITB exit profiles. An eddy-dissipation approach was used to account for turbulence-chemistry interaction.

4. Numerical Simulation Scheme

A pressure based implicit steady state formulation with Green-Gauss node based gradient evaluations was utilized due to mesh element types and expected Mach number range. The Realizable k-e model with non-equilibrium wall functions was used to model the effects of turbulence. It should be noted that the mesh was constructed to be consistent with the desired wall Y+ for this model. The discrete phase was set to interact with the continuous phase every 20 iterations. The saturation vapor pressure for kerosene was set to be piecewise-linear, and the Cp was set to be piecewise-polynomial for the continuous phase species. All other material properties were set to default values.

5. Boundary Conditions

Figure 2 shows a 360-degree schematic of the ITB configuration with four radial vanes and the imposed boundary conditions. The geometry is 180 degree periodic, however it was not feasible to generate a face matched periodic mesh surface for the highly curved and irregular periodic region. The fuel is injected into the cavity normal to the axial flow direction using a cone injector with a 35 degree half angle, a radius of 0.0014 meters, a temperature of 290K, a rosin-rammler distribution, a velocity of 23.18 meters per second (m/s), a mass flow of 0.0002898 kilograms per second (kg/s) per injector, a minimum diameter of 1e-07 m, a maximum diameter of 3e-05 m, a mean diameter of 1.5e-05 m, a spread parameter of 3.5, 500 streams and 30 diameters, and stochastic tracking. The fuel is injected into the cavity at six equally spaced points around the circumference of the cavity such that only six fuel injectors would be required for the 360 degree sector as shown in Figure 2. Air flow is injected into the cavity at 45 and 30 degree angles from 24 ports. Non-vitiated air is admitted axially as main airflow. The main airflow interacts with the circumferential cavity combustion products. In this investigation the airflow split between the main and the circumferential cavity is respectively about 85% and 15% of the 0.1775 kg/s total airflow. Main and cavity airflow pressure drops were about 3%. At the inlet boundary, conditions were specified for static temperature, pressure, oxygen and nitrogen mass fractions for non-vitiated air, and mass flow. At the exit, based upon the outflow characteristics, only the static pressure at the ITB exit plane needs to be imposed for subsonic exit flows. The remaining exit parameters are extrapolated from the interior domain. Mass flow rates and flow properties are summarized in Tables 1 and 2. All solid walls are treated as no slip with zero heat flux.

6. Computational Grid

A 360-sector grid for ITB design configuration is shown in Figure 3. The mesh contains 4 million mixed element computational cells. Several runs were performed with various wall field spacing parameters. A wall cell normal distance of 0.9 mm with a growth rate of 1.1 was selected for a target Y+ of 50–300 and smooth cell size variation. Examination of preliminary results provided a visual indication that the mesh was adequate to resolve the flow features. Separate faces were created for the twenty-four air flow ports with conformal boundary curves. Overall grid spacing was adequate to resolve viscous boundary layers. All surface meshes were constructed using GRIDGEN[23]. These surface meshes were output, and AFLR3D[24] was used for volume mesh generation. Several preliminary meshes exhibited numerical instability and great care was exercised to provide maximum grid quality in terms of cell equiangle and equivolume skew to eliminate the numerical instability. Once a mesh was constructed that yielded stable converged and visually pleasing results, simulations were undertaken with 1^{st}-, 2^{nd}-, and 3^{rd}-order discretization schemes. The 3^{rd}-order ran for several thousand steps from a converged 2^{nd}-order restart file before developing an instability. However there was little qualitative variation on the predicted flow structures and temperature distributions. Preliminary results for a solution adaptive mesh of 5 million cells have also been obtained. The qualitative flow structures are very similar to the base mesh with differences near the top and bottom fuel injectors and the blade cavities feed by these injectors. Based upon this analysis, it is believed that the current mesh provided adequate resolution for the purpose of this study.

Table 1 contains the operating conditions for the ITB curved radial vane design configuration. Pressure operating condition is atmospheric, but the main airflow is non-vitiated and is heated to 533K. The circumferential cavity operating fuel-air ratio is rich whereas the overall fuel-air ratio is very lean. The operating conditions were utilized to set up the boundary conditions for the ITB simulations. Tables 2 gives the boundary conditions imposed on the computational domain boundaries.

Table 1

Operating Pressure (atm)	Inlet Temperature (K)	Main Airflow Rate (kg/s)	Cavity Airflow Rate (kg/s)	Total Airflow Rate (kg/s) (kg/s)	Overall Equivalence Ratio
1.0	533	1.4946×10^{-1}	2.8063×10^{-2}	1.7752×10^{-1}	0.01

Table 2

Main Inlet Airflow Temperature (K)	Main Inlet Airflow Gage Pressure (Pa)	Cavity Airflow Gage Pressure (Pa)	Cavity Fuel Flow Rate (kg/s)	Cavity Airflow Inlet Temperature (K)	Main Airflow Turbulence Intensity (%)	Main Airflow Turbulence Length Scale (m)	Spray SMD (μm)	Spray Injection Velocity (m/s)
533.15	3268.5	3268.5	1.738×10^{-3}	533.15	3.0	0.025	15.0	23.18

The figures and grids demonstrate the CRV with the cavity situated in the suction side of the vane as shown in Figure 4a. Figures 4b and 4c show the location of the vane cavity in the pressure side and a CRV with no vane cavity.

Figures 5a–5e shows the air injection direction in the circumferential cavity with respect to the CRV. Regardless of the air injection direction, the direction and parameters defining the liquid fuel injection are kept constant.

7. CFD Results and Discussion

Figures 6a–6h show the predicted temperature distribution, axial, radial, tangential, total velocity magnitude, velocity vectors in the XY plane, $C_{12}H_{23}$ distribution, and CO_2 distribution at several stations along the ITB configuration. A 3D overview is shown with the two-dimensional (2D) axial sections in the r-θ planes for the for suction side counter clockwise (SS-CCW) case. Significant interaction between main and circumferential cavity airflows occurs largely through the shear layer and vane's radial cavity. The main airflow gets entrained in the radial vane cavity as a result of flow interaction due to the curvature effects of the radial vane, the increase in the circumferential cavity tangential flow velocity, and the air jets which impinge near the leading edge of the radial vanes. As the main airflow approaches the leading edge of the RVC, it separates near the leading edge, reattaches and fills in near the rear end of the cavity, and then bounces out of the cavity at a relatively large angle in the circumferential direction as clearly visible in Figure 6b and 6e for the axial and total velocities.

Low axial velocity in the RVC is evident, particularly near its leading edge. Flow shedding from the RVC occurs at the downstream end of the cavity. However, the dominant mechanism for the circumferential cavity airflow entrainment into main stream is seen to occur through the RVC. As the combustion products flow from the circumferential cavity into the RVC, the main stream detaches from the leading edge of the RVC and flows into the hot products, entrained in the cavity to mix there with combustion products and deflects back into the main airflow passage after it is reattached in the cavity. The presence of the downstream side of the RVC causes the entrained main airflow to mix with the cavity hot products further. The axial velocity field in the circumferential cavity shows minor variations indicating diminished axial motion in the cavity.

The predicted radial velocity field, as shown in Figure 6c shows important variations in the circumferential cavity. In addition, the flow structure in the RVC induces changes in the radial velocity in the circumferential cavity. The importance of the radial velocity behavior in the circumferential cavity can be critical for determining the rate of entrainment into the main airflow of the circumferential cavity combustion products. This is very much dependent on the fuel injection and air injection angle.

As shown in Figure 6h, the vaporized fuel spreads across the circumferential cavity with the highest concentration occurring in the proximity of the fuel injector and along the RVC. Due to the cavity swirling flow, the fuel vapor distribution is predicted to be highly non-uniform, and remains in the RVC due to the suction pressure in the region of RVC placement. Fuel vapor can be seen on the suction side of the vane. The swirling cavity airflow reduces the fuel jet penetration into the circumferential cavity and substantially alters the fuel injection cone angle. This finding is important for optimizing the fuel vapor distribution in the cavity and its diffusion into the vane's radial cavity. Lean burning can occur in the RVC. The predicted fuel vapor mass

fractions clearly point out that based on the predicted fuel vapor in the circumferential cavity, rich burning would take place in the circumferential cavity. Higher fuel vapor jet penetration is required for improving fuel-air ratio distribution and consequently combustion. Figure 6a exhibits the predicted temperature contours respectively along the UCC/ITB flow path, at various axial locations. Higher temperatures are predicted in the circumferential cavity in the proximity of the fuel injector and spreading of the burning zone across the cavity in the tangential direction is non-uniform. Overall, this appears to improve the radial transport of the hot products inwards towards the radial cavity. A number of hot burning regions seem to develop in the RVC. The burning region develops near the shear layer between the main and cavity flows and extends across the entire cavity and temperature distribution suggest proximity of the fuel injection point dictates the temperature distribution in the circumferential direction and on the RVC. The higher temperature spot occurs on the RVC side, which is close to the fuel injector location.

The predicted temperature field also shows that combustion products transported into the RVC and main stream is distributed. Figures 6a clearly depicts the extent to which the combustion products mix with the main airflow. Combustion products are predicted to migrate axially along the shear layer with moderate radial migration towards the vane's hub. The temperature distribution appears to be more uniform further along the downstream of the radial vane cavity. The results show that a sizable portion of the main airflow remains undisturbed near the hub. This may be due to the large angle of the hub towards the exit. It is observed at the exit of the ITB, there is found to be upstream interaction due to reversed flow. It is believed the flow does not attach to the center body until the exit.

Figure 6g illustrates the predicted CO_2 mass fraction contours at various stations along the ITB flow path. It can be seen that the predicted CO_2 field is qualitatively similar to the temperature field as shown in Figure 6a. The highest CO_2 and H_2O concentrations occur in the hot burning zones. The circumferential cavity airflow jets have relatively high penetration which seems to quench the high temperature burning zone across the cavity at discrete locations and result in lowering the production rate of combustion products. On the other hand, the airflow jets are seen to quench segments of the cavity's flame, thereby decreasing the combustion rate and increasing the chemical time.

Figure 7 shows the temperature distribution and CO_2 distribution at the exit. The migration mechanism by which the combustion products are transported from the circumferential cavity to main stream is seen to be adequate for obtaining high quality temperature profile at the exit plane. The exit temperature and the product CO_2 distribution for the three cases, namely, suction side clockwise (SS-CC), SS-CCW, and no cavity in vane (NN), as shown in Figure 7 clearly illustrates the effect of suction side vane cavity with the air injection in the counter-clock-wise direction offers an almost desired profile, as evidenced in the mass averaged profile, as shown in Figure 9. Similar pictures for the pressure side (PR-CCW), PR-CW have also been examined. Figure 8 shows the velocity vectors, colored by the temperature at three selected axial planes, within the circumferential cavity at three planes for all the configurations, studied, namely SS-CW, SS-CCW, NN, PR-CW, and PR-CCW. In the PR-CW and SS-CW, there is a pocket of recirculating flow between the vanes, which is not present in the PR-CCW and SS-CCW. One would clearly see the effect of these vane shapes and the air flow direction on the entrainment. Finally, the mass averaged temperature profile at the exit station of the ITB for all the RCV SS-CCW, SS-CW, PR-CCW, PR-CW, and NN configurations are shown in Figure 9. These profiles were obtained by mass averaging in the tangential direction. The predicted exit temperature values at a number of radial locations along the turbine vane span, as would normally be done to obtain temperature radial profile in conventional combustors, were used for mass averaging..

The peak exit temperature for SSW-CCW occurs at the vicinity of the mid span, is about 950K for an fuel/air (F/A) ratio of 0.01 and inlet temperature of 533K at atmospheric pressure conditions. The SS-CW and PR-CW exit profiles are peaking near the hub, while PR-CCW and NN profiles are peaking out in the center of the RCV. From the exit profiles obtained, one would see the SS-CCW radial curved vane exit temperature profile is a much more desirable exit profile for downstream turbine stages, than the temperature profile for the PR-CCW, PR-CW, SS-CW, and NN. Only a limited post processing of the obtained flow field has been carried out. The complexity of the geometry requires that we find new methods of visualizing this sort of voluminous and complex flow field data. Simultaneously rig tests on these configurations are currently taking place. As soon as the experimental data is reduced, these calculations will be repeated for the exact experimental conditions and will be reported in the succeeding papers. This work is aimed towards a preliminary investigation on determining the type of exit profiles, one would expect when various configurational changes are implemented in the CRV. Figure 10 shows the total pressure loss, normalized with respect to the approaching flow total pressure calculated from these computations. The actual values appear to be on the higher side. But the calculated values of the total pressure loss in terms of percentage loss gives a trend of the losses of each configuration.

8. Conclusion

Three-dimensional two-phase CFD analysis by FLUENT has been used to numerically investigate the turbulent combusting flow field inside an AFRL UCC/ITB curved radial vane design concept under atmospheric pressure conditions. The gas-phase equations for mass, momentum, energy, chemical species, and turbulence were solved using a finite-volume methodology. A liquid fuel-spray was injected and was modeled by selecting an initial droplet size, location, velocity, and temperature and using a droplet size distribution. A one-step global irreversible reaction scheme was used to model the finite-rate kinetic of Jet-A fuel. High Reynolds number turbulent kinetic energy and its dissipation rate k-ε were employed to model turbulence along with a non equilibrium wall function for the solid walls. The CFD results indicated that multiple combustion zones developed in the high-g loaded cavity and this was attributed to the airflow jets penetration inside the cavity. Intense combustion inside the cavity, located on the suction side of the RVC was also predicted. The hot combustion products were predicted to migrate from the cavity to main airflow through the shear layer with good mixing with the main airflow in the combined mode of radial-tangential transport in the downward direction. The curved RVC was modeled with a cavity in the suction side, pressure side, no cavity and injected air from the circumferential cavity in both clockwise and counter clock wise direction. Overall, the RVC was useful in transporting circumferential cavity flow to mix with the main airflow. The direction of the air injection into the circumferential cavity is a critical parameter for determining the shape of exit profile. The SS-CCW performs better, compared to the PR-CCW and NN configuration. The SS-CW and PR-CW perform poorly. The CFD analysis also indicated that robust mixing of combustion products with the main airflow, resulted in radial temperature profile peaks at the central portion of the ITB exit as desired, except for the SS-CW and PR-CW configurations. This study shows that the temperature profile obtained with the RVC in the SS-CCW is superior. The present CFD analysis thus has identified the potential of the RVC design. The mixing of cavity combustion products with the main airflow in the considered ITB RVC design configuration could be even further enhanced to produce an improved temperature field and radial profile at the ITB exit, by altering and optimizing the air injection schemes and fuel injection schemes. This warrants further CFD investigations and more experiments.

Acknowledgements

The results supporting this publication were made possible through support provided by the DoD High Performance Computing Modernization Program. The authors would like to thank Mr. Jack Yoder of Innovative Science Solutions, Inc. for the development and modification of the computer-aided design models, as well support for the translation of such models into a neutral format.

References

1. Horlock, J.H., *Combined Power Plants*, Pergamon Press, 1992.

2. Stodola, *Dampf und Steam Turbine (Gas and Steam Turbines)*, 2nd Edition, 1927, translation by McGraw-Hill, 1924.

3. Rolf Kehlhofer, R., (Editor), *Combined - Cycle Gas & Steam Turbine Power Plants*, 1999.

4. Boyce, M.P., *Handbook for Cogeneration and Combined Cycle Power Plants*, 2000.

5. Harris, F.R., "Reheat in Early Gas Turbines." *Historical Note, Proceedings of the Institute of Mechanical Engineers, Part A*, Volume 208, 1994.

6. Crane, R.I., "A Critical Analysis of the Thermodynamic Advantages of Reheat in Gas Turbines." *Proceeding of the Institute of Mechanical Engineers, Part A*, Volume 212, 1998.

7. Kerrebrock, J.L., *Aircraft Engines and Gas Turbines*, MIT Press, 1992.

8. Sirignano, W.A., J.P. Delplanque, et al., "Selected Challenges in Jet and Rocket Engine Combustion Research." *AIAA-97-2701*, 33rd AIAA/ASMESAE/ASEE Joint Propulsion Conference, Seattle, WA, 1997.

9. Sirignano, W.A., and F. Liu, "Performance Increases for Gas-Turbine Engines Through Combustion Inside the Turbine." *Journal of Propulsion and Power*, Volume 15, Number 1, pp.111–118, January/February 1999.

10. Liu, F., and WA. Sirignano, "Turbojet and Turbofan Engine Performance Increases Through Turbine Burners." *AIAA-2000-0741*, 38th Aerospace Sciences Meeting & Exhibit, Reno, NV, 2000.

11. Volger, K., "The Potential of Sequential Combustion for High Bypass Jet Engines." *98-GT-311*, Turbo-Expo 1998, 1998.

12. Andriani, R., U. Ghezzi, and L. Ferri, "Jet Engines with Heat Addition During Expansion." 37th AIAA, Aerospace Sciences Meeting, January 11–14, 1999, Reno, NV, USA, 1999.

13. Zelina, J., J. Ehret, R.D. Hancock, D.T. Shouse, and W.M. Roquemore, "Ultra-Compact Combustion Technology Using High Swirl for Enhanced Burning Rate." *AIAA Paper 2002-3725*, 38th Joint Propulsion Conference & Exhibit, Indianapolis, IN, 7–10 July 2002.

14. Zelina, J., T. Shouse, and R.D. Hancock, "Ultra-Compact Combustors for Advanced Gas Turbine Engines." *ASME IGTI Paper 2004-GT-53155*, Vienna, Austria, June 2004.

15. Zelina, J., G.J. Sturgess, A. Mansour, and R.D. Hancock, "Fuel Injection Design for Ultra-Compact Combustor." *ISABE-2003-1089.*

16. Zelina, J., G.J. Sturgess, and D.T. Shouse, "The Behavior of an Ultra-Compact Combustor (UCC) Based on Centrifugally-Enhanced Turbulent Burning Rates." AIAA Paper 2004-3541.

17. Mawid, M.A., T.W. Park, H. Thornburg, B. Sekar, and J. Zelina, "Numerical Analysis of Inter-Turbine Burner (ITB) Concepts for Improved Gas Turbine Engine Performance." *AIAA Paper 2005-1162*, 43rd AIAA Aerospace Sciences Meeting and Exhibit, Reno, NV, 10–13 Jan. 2005.

18. Mawid, M.A., H. Thornburg, B. Sekar, and J. Zelina, "Prediction of Inter-Turbine Burner (ITB) performance with vitiated air-stream." *ISABE -2005-1022.*

19. Mawid, M.A., H. Thornburg, B. Sekar, and J. Zelina, "Performance of an Inter-Turbine Burner (ITB) Concept with Three Different Vane Cavity Shapes." *AIAA 2006-4740*, 42nd AIAA/ASME/SAE/ASEE Joint Propulsion Conference, Sacramento, CA, July 2006.

20. Zelina, J, D.T. Shouse, J.S. Stutrud, G.J. Sturgess, and W.M. Roquemore, "Exploration of Compact Combustors for Reheat Cycle Aero Engine Applications." *GT 2006-90179*, Barcelona, Spain, May 2006.

21. Zelina, J., R.T. Greenwood, and D.T Shouse, "Operability and Efficiency of Ultra-Compact High Gravity (g) Combustor Concepts." *GT 2006-90119*, Barcelona, Spain, May 2006.

22. *FLUENT 6.3.21*, www.fluent.com.

23. *Pointwise, Inc.*, GRIDGEN V15, 2004.

24. *AFLR3D*, www.erc.msstate.edu.

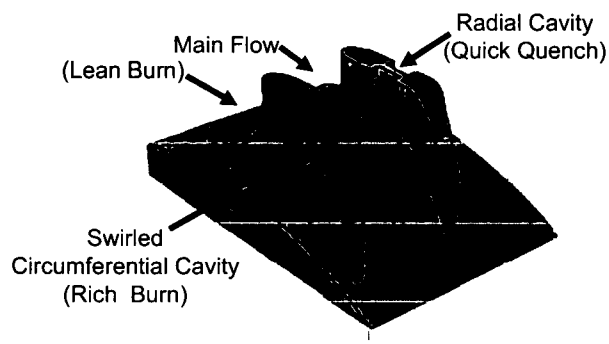

Figure 1. UCC baseline ITB concept for advanced combustion systems

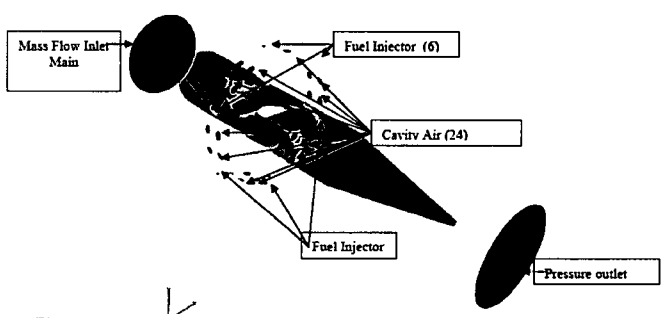

Figure 2. A 360-degree sector schematic with boundary conditions

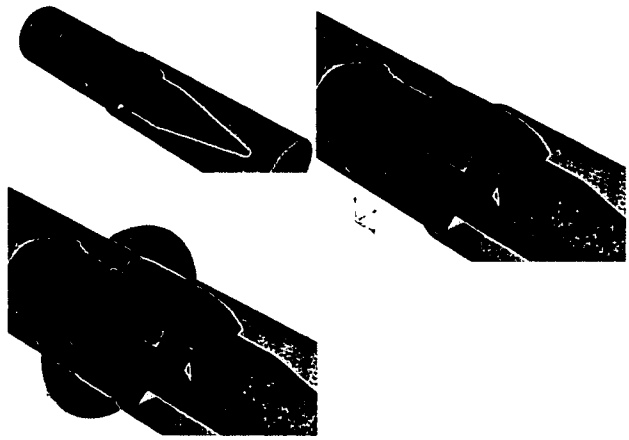

Figure 3. Hybrid computational grid (4,052,623 cell) for ITB design

Figure 4a. Schematics of the CRV configuration UCC/ITB with cavity in the suction side of the vane

Figure 4b and 4c. Schematics of the CRV configuration UCC/ITB with cavity on the pressure side of the vane and with no cavity

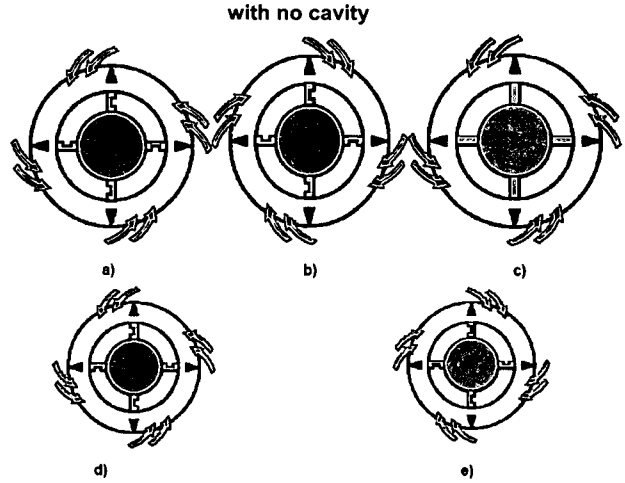

Figure 5. Nomenclature of the modeled cavity radial vane. a} Cavity on the suction side, counter-clock wise air injection (SS-CCW) – looking upstream; b) cavity on the suction side, clockwise air injection, (SS-CW) – looking upstream; c) no cavity in the vane, (NN)- looking upstream; d) Cavity on pressure side, counter-clock wise air injection (PS-CCW) – looking upstream; and e) Cavity on pressure side, clock wise air injection (PS-CCW) – looking upstream.

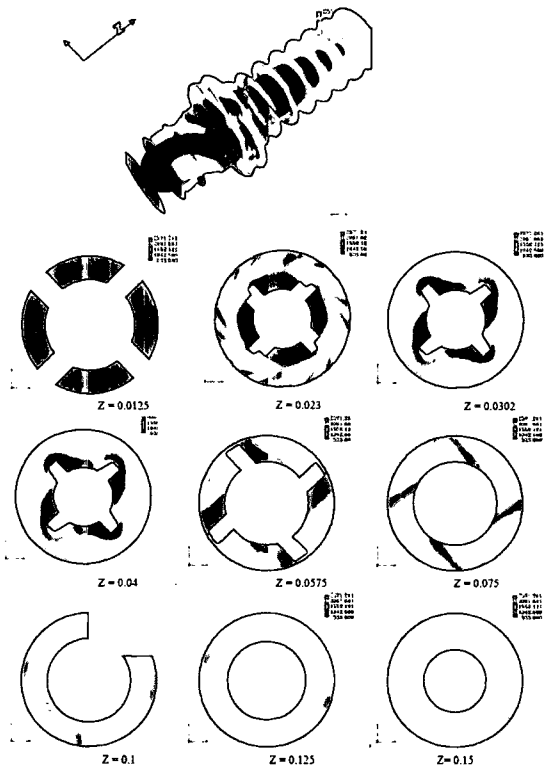

Figure 6a. Predicted temperature contours along the flow path

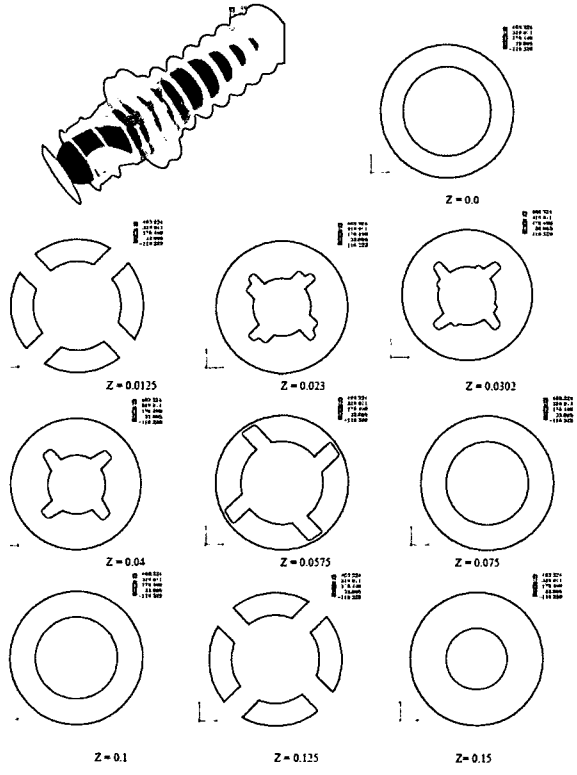

Figure 6b. Predicted axial velocity contours along the flow path

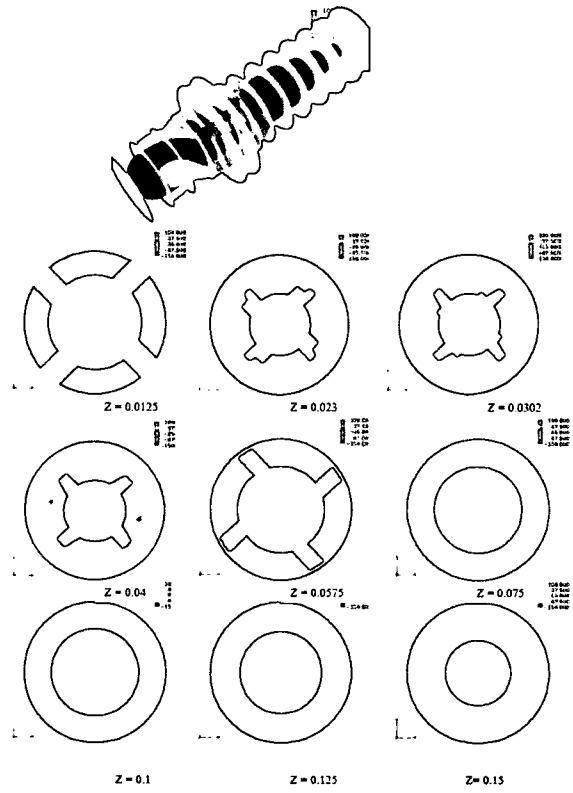

Figure 6c. Predicted radial velocity contours along the flow path

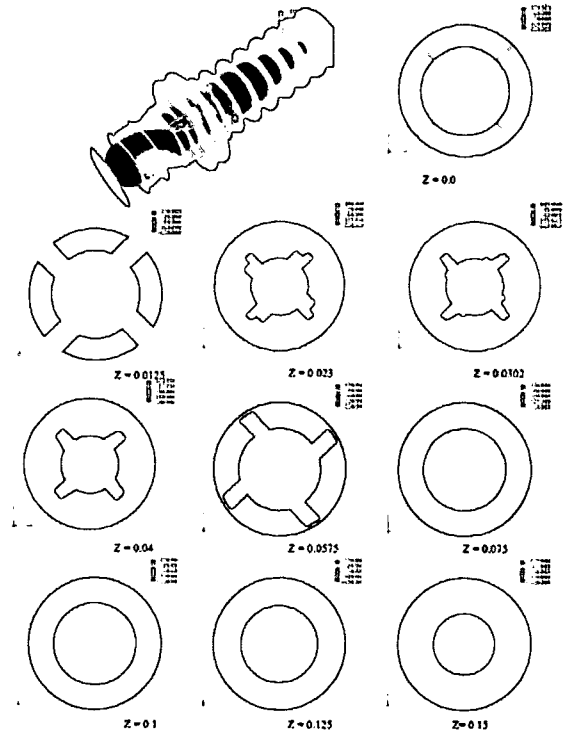

Figure 6d. Predicted tangential velocity contours along the flow path

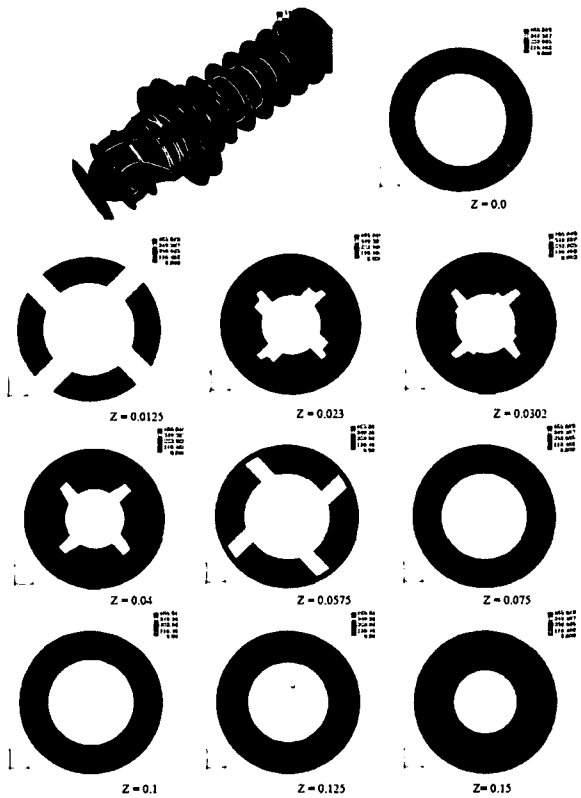

Figure 6e. Predicted total velocity contours along the flow path

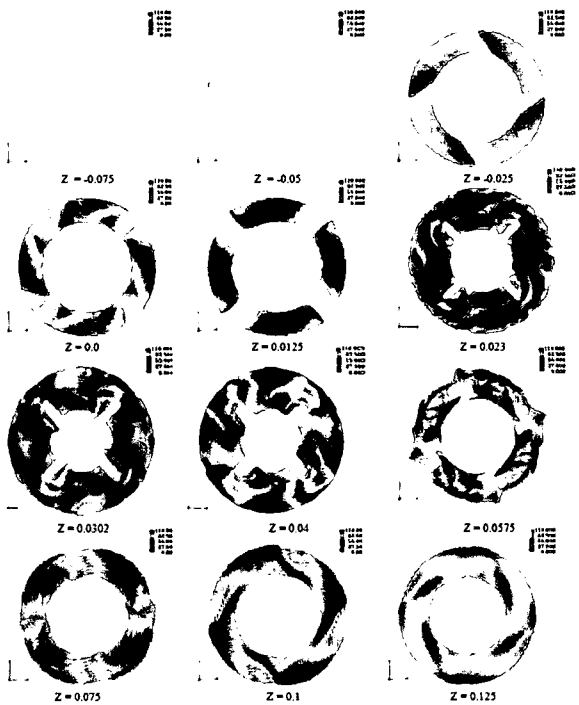

Figure 6f. Predicted 2D (X,Y) velocity vectors along the flow path

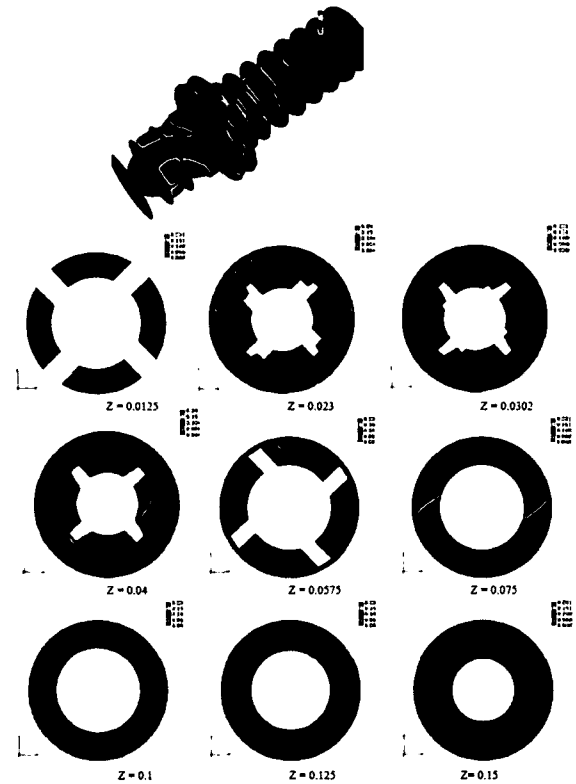

Figure 6g. Predicted CO_2 contours along the flow path

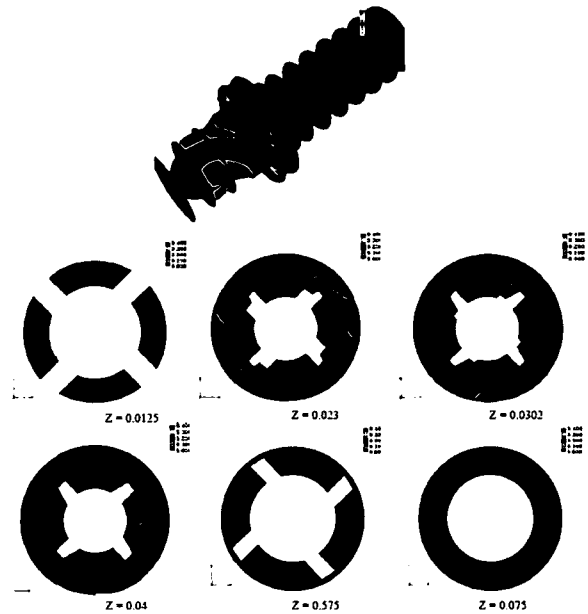

Figure 6h. Predicted $C_{12}H_{23}$ contours along the flow path

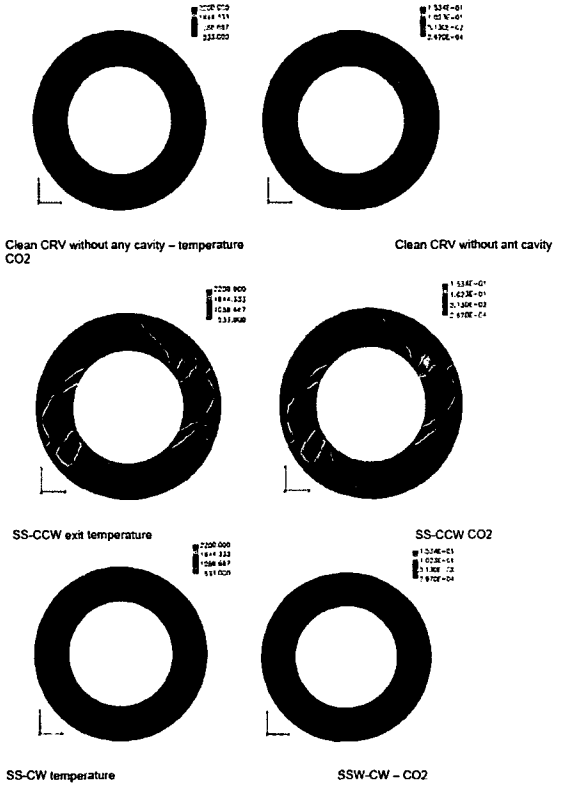

Figure 7. The exit temperature and CO_2 distribution, for the configurations SS-CW, SS-CCW and NN

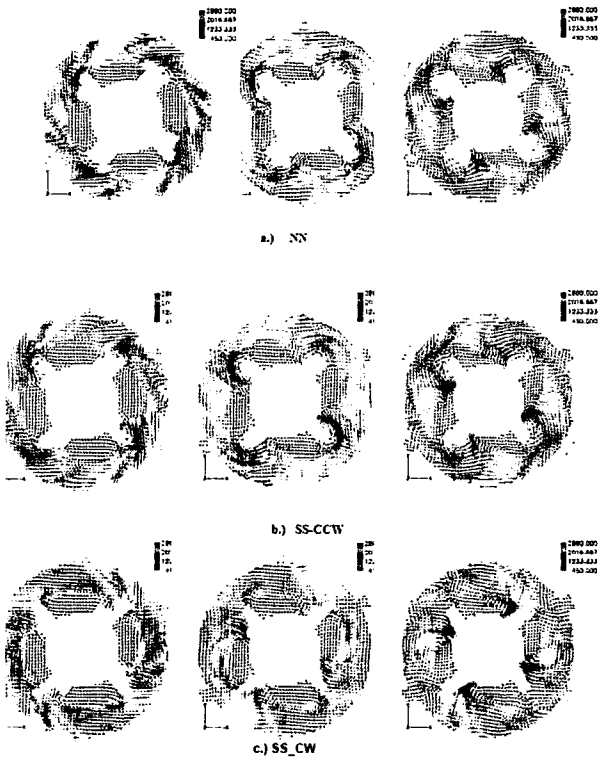

Figure 8 a–c. Predicted 2D (X,Y) velocity vectors colored by temperature

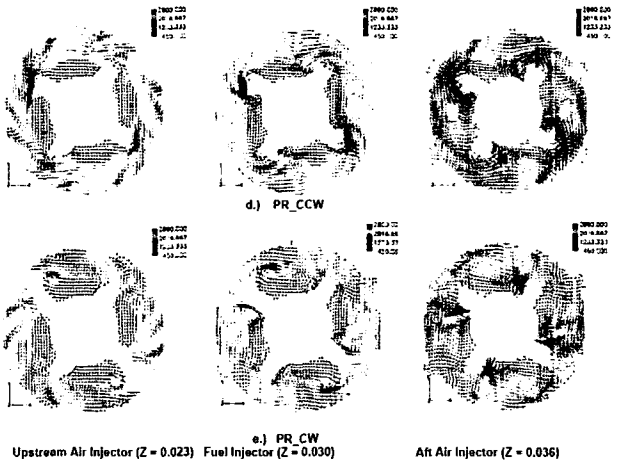

Figure 8 d–e predicted 2D (X,Y) velocity vectors colored by temperature

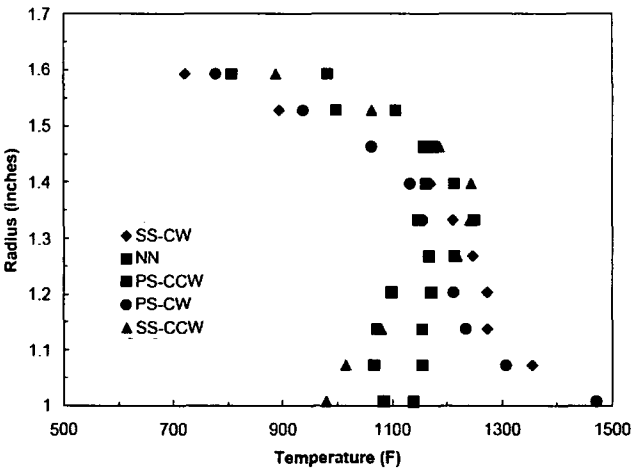

Figure 9. Comparison of mass averaged exit temperature profiles for the curved radial vane configurations SS-CCW, SS-CW, PR-CW, PR-CCW and NN

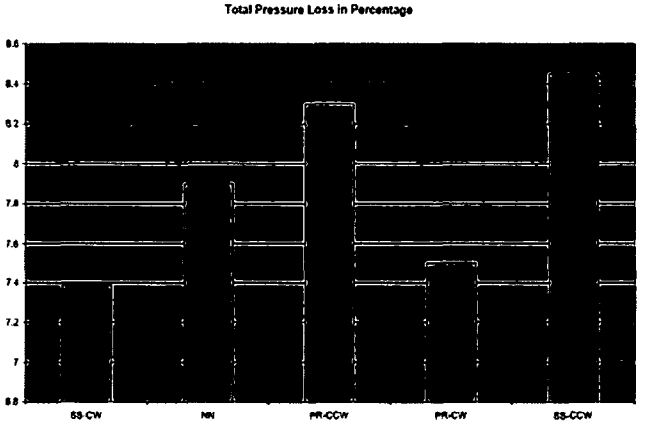

Figure 10. Comparison of total pressure losses